COMPDYN 2013
4th ECCOMAS Thematic Conference on
Computational Methods in Structural Dynamics and Earthquake Engineering
M. Papadrakakis, V. Papadopoulos, V. Plevris (eds.)
Kos Island, Greece, 12–14 June 2013

ON OPTIMUM DESIGN AND PERIODICITY OF BAND-GAP STRUCTURES

Niels Olhoff[1], Bin Niu[1], and Gengdong Cheng[2]

[1] Department of Mechanical and Manufacturing Engineering, Aalborg University,
Fibigerstraede 16, DK-9220 Aalborg East, Denmark
e-mail: {no, bni}@m-tech.aau.dk

[2] State Key Laboratory of Structural Analysis for Industrial Equipment,
Dalian University of Technology, 116024 Dalian, China
chenggd@dlut.edu.cn

Keywords: Band-gap Structures, Optimum Eigenfrequency Gap, Periodic Structures.

Abstract. *A band-gap structure usually consists of a periodic distribution of elastic materials or segments, where the propagation of waves is impeded or significantly suppressed for a range of external excitation frequencies. Maximization of the band-gap is therefore an obvious objective for optimum design. This problem is sometimes formulated by optimizing a parameterized design model which assumes periodicity in the design. However, it is shown in the present paper that such an a priori assumption is not necessary since, except for regions adjacent to the structural boundaries, the maximization of the band-gap alone, generally leads to significant design periodicity.*

This paper extends earlier optimum shape design results for transversely vibrating Bernoulli-Euler beams by determining new optimum band-gap beam structures for (i) different combinations of classical boundary conditions, (ii) much larger values of the orders n (n>1) and n-1 of adjacent upper and lower eigenfrequencies of maximized band-gaps, and (iii) different values of a minimum beam cross-sectional area constraint.

In the present paper, instead of maximizing band-gaps between frequencies of propagating waves or forced vibrations excited by external time-harmonic loads, the closely related problem of maximizing the gap between two adjacent eigenfrequencies ω_n and ω_{n-1} of any given consecutive orders n (n>1) and n-1, is considered. This is justified by the fact that external time-harmonic dynamic loads cannot excite resonance with high vibration levels of standing waves, if the eigenfrequencies of the structure are moved outside the range of the external excitation frequencies by the optimization.

Finally, the present study shows that if an infinite beam structure is constructed by repeated translation of an inner beam segment obtained by the aforementioned frequency gap optimization, then a band-gap of traveling waves in this infinite beam is found to correlate almost perfectly with the maximized frequency gap in the finite structure.

1 INTRODUCTION

A band-gap structure can quench vibrations and significantly suppress the propagation of waves for a certain range of frequencies. Such a frequency range is termed a band-gap or stop-band. The phenomenon may occur for elastic, acoustic or electromagnetic waves, see Refs. [1-6]. Except for regions close to the boundaries, a band-gap structure usually consists of a periodic distribution of different elastic materials, or repeated identical segments if a single elastic material is prescribed for the structure. Due to a wealth of potential applications in vibration protection, noise isolation, waveguiding, etc., the study and development of band-gap rod, mass-spring, beam, grillage, disk and plate structures, in most cases by topology optimization, have attracted increasing attention in recent years, see e.g. [5,7-18]. Elastodynamics of finite or infinite periodic 1D rod or beam structures has been studied in [6, 19-21]. Comparisons between Floquet theory ([1]) based unit cell analysis of a band structure and the vibration response analysis of the corresponding finite periodic structure, are presented in [22] for one-dimensional diatomic chains of uncoupled spheres and in [14] for 1D rod structures, respectively.

The problem of design optimization of various types of structures for maximum value of a natural frequency or maximum gap between two adjacent natural frequencies is extensively studied, see, e.g., [23-27] for shape optimization of beam structures, and reference may be given to, e.g., [12,15,16,28,29] for topology optimization of continuum structures, and to [30] for two-scale topology optimization of continuum structures with microstructures. An abundance of other references is available in the exhaustive textbook [31]. The problem of minimization of forced vibration response of structures subjected to external time-harmonic loading has been studied in, e.g., [7,17,29,32-34].

The present paper is based on recent work [35]. Instead of maximizing band-gaps between frequencies of propagating waves or forced vibration excited by external time-harmonic loads, we shall consider the closely related problem of maximizing the gap (also called the separation or difference) between two adjacent natural frequencies (synonym: eigenfrequencies) of free vibration modes (synonym: eigenmodes) of appropriate orders. Note that external time-harmonic dynamic loads cannot excite resonance phenomena with high vibration levels associated with standing waves, if the eigenfrequencies of the structure are moved outside the range of the excitation frequencies of the dynamic loading by the design optimization. We demonstrate that maximization of the frequency gap leads to significant design periodicity. Moreover, the present paper also shows that if an infinite beam structure is constructed by repeated translation of an inner beam segment obtained in the frequency gap optimization above, a band-gap of traveling waves within this infinite periodic beam matches very well with the maximized frequency separation. Thus, the problem of maximizing band-gaps between frequencies of standing or propagating waves can be solved by considering the problem of maximizing the separation between two adjacent eigenfrequencies of free vibration modes of given order.

To the authors' best knowledge, Refs. [24,26,27] were the first publications on problems of optimizing vibrating structures for maximum frequency gap – *albeit* the term difference (or separation) between adjacent natural frequencies (eigenfrequencies) was used rather than the term frequency gap in these papers.

As in the current paper, the structures considered in the papers just cited are thin, elastic, transversely vibrating Bernoulli-Euler beams without damping, and the problems are considered in non-dimensional form. The beams are subjected to shape optimization with the cross-sectional area function as design variable, and no assumption of periodicity is imposed. The cross-sections are assumed to be geometrically similar (e.g. circular), and the total

volume, length and boundary conditions of the beams are assumed to be given.

In fact, Ref. [24] considers the problem of optimizing Bernoulli-Euler beams with any combination of free, simply supported or clamped ends for maximum value of an eigenfrequency ω_n of any prescribed order n, n = 1, 2, 3, …., (see also Section 2), without specifying a minimum constraint for the variable cross-sectional area, thereby allowing vanishing cross-section of the optimized beams. The latter implies that a beam optimized with respect to a higher-order eigenfrequency ω_n (n >1) will turn out to possess n-1 degrees of inner kinematic freedom to perform *rigid-body motions* due to the formation of points of vanishing beam cross-section. At these points, either *inner beam separations* with both zero shear force and bending moment, or *inner hinges* of zero bending moment (but finite shear force) are created in such a way that all the n-1 rigid-body eigenfrequencies $\omega_1, \ldots, \omega_{n-1}$ below the maximized n-th eigenfrequency ω_n reduce to zero.

Thus, without the specification of a minimum cross-sectional area constraint, [24] presents results that simultaneously constitute solutions to the problem of maximizing the n-th eigenfrequency ω_n and the problem of maximizing the gap $\omega_n - \omega_{n-1}$ between the n-th and the (n-1)-th eigenfrequencies of the beams. It should be borne in mind that these solutions must be considered as optimum, *limiting* solutions from the point of view of practical design.

In [24], the governing equations are derived by the calculus of variations and solved numerically by a successive finite difference technique based on a formal integration of the problem for relatively low values of the given order n of the eigenfrequency ω_n. For any higher value of n, the inner beam separations make it possible to solve very easily the maximum ω_n and the maximum $\omega_n - \omega_{n-1}$ problems (including the determination of the corresponding optimum beam designs) with the aid of a very simple quasi-analytical method of "Scaled Optimum Beam Elements" developed in [24]. Thus, it may be stated that for beams with any combination of the classical beam end boundary conditions mentioned above, the optimum solutions corresponding to any given value of n are presented in [24]. These early frequency gap beam results clearly show that already starting at moderate values of n, say n=5, the optimum beam designs exhibit a periodicity that increases significantly with increasing values of n.

In contrast to the paper just discussed, a minimum cross-sectional area constraint (prohibiting creation of inner beam separations and hinges), was taken into account in the follow-up papers [26,27] which present two slightly different mathematical formulations of the problem of directly maximizing the eigenfrequency gap $\omega_n - \omega_{n-1}$ for cantilever beams. The beams are optimized with and without attached non-structural masses, and numerical results are presented for values of n up to 5.

The present paper aims to highlight and extend design results obtained in [24, 26,27] by determining and presenting new optimum frequency gap beam structures in non-dimensional form for (*i*) different combinations of classical boundary conditions, (*ii*) much larger values of the orders n and n-1 of the adjacent upper and lower eigenfrequencies of maximized frequency gaps, and for (*iii*) different values of a positive minimum cross-sectional area constraint. The new results are obtained by finite element and gradient based optimization using analytical sensitivity analysis. The new solutions are compared with corresponding limiting optimum solutions obtained without minimum cross-sectional area constraint by usage of the aforementioned method of "Scaled Optimum Beam Elements" developed in [24].

The remainder of this paper is organized as follows. First, the optimization formulation of maximizing gaps between adjacent eigenfrequencies is presented in Section 2. Section 3

presents sensitivity analysis results and an incremental numerical procedure for solutions of the optimization problems. In Section 4, several numerical examples are presented and discussed. Section 5 contains a discussion of interesting characteristics of the problem when considered in geometrically unconstrained form. In Section 6, a repeated inner segment of the optimized beam is analyzed via Floquet theory and the waveguide finite element (WFE) method to identify the pass-bands and stop-bands of traveling waves. Subsequently, forced vibration of the optimized beam subjected to an external time-harmonic excitation is performed to study the vibration filter effect of the optimized periodic beam. Finally, observations and conclusions are drawn based on the optimization results.

2 FORMULATION FOR MAXIMIZING GAPS BETWEEN ADJACENT EIGENFREQUENCIES FOR BEAM STRUCTURES

Bernoulli-Euler beams of given length L, and volume V are considered for the frequency gap optimization problem, where only free, transverse vibration frequencies (eigenfrequencies) and associated modes (eigenvectors) are included. The beams are made of a linearly elastic material with Young's modulus E and mass density γ, and have variable, but geometrically similar (e.g., circular) cross-sections with the relation $I = cA^2$ between the area moment of inertia I and the cross-sectional area A. The constant c is given by the cross-sectional geometry.

By introducing a dimensionless coordinate $x = X/L$, $0 \le x \le 1$ and cross-sectional area function $\alpha(x) = A(x)L/V$ along the beam, the dimensionless n-th eigenvalue λ_n ($\lambda_n = \omega_n^2$, where ω_n is the dimensionless circular eigenfrequency) associated with free, transverse vibrations takes the form [24]

$$\lambda_n = \omega_n^2 = \frac{\bar{\omega}_n^2 \gamma L^5}{cEV}, \tag{1}$$

where $\bar{\omega}_n$ is the dimensional n-th circular eigenfrequency of the given beam.

In a dimensionless finite element setting where the non-dimensional length and volume of the beam are both assigned unit value, the problem of design optimization with the objective of maximizing the gap between two adjacent frequencies ω_n and ω_{n-1} of given orders n and n-1, can be formulated as follows:

$$\begin{aligned}
&\max_{\alpha_e} \left\{ \Delta(\omega^2) = \omega_n^2 - \omega_{n-1}^2 \right\} && (a)\\
&\text{subject to}\\
&\mathbf{K}\boldsymbol{\phi}_j = \omega_j^2 \mathbf{M}\boldsymbol{\phi}_j,\ j = 1, \ldots, J, && (b)\\
&\boldsymbol{\phi}_j^T \mathbf{M}\boldsymbol{\phi}_k = \delta_{jk},\ j, k = 1, \ldots, J, && (c)\\
&\sum_{e=1}^{N_E} \alpha_e l_e - 1 \le 0, && (d)\\
&0 < \alpha_{\min} \le \alpha_e,\ e = 1, \ldots, N_E. && (e)
\end{aligned} \tag{2}$$

Here, ω_j and $\boldsymbol{\phi}_j$ are the dimensionless j-th eigenfrequency and corresponding eigenvector, respectively, and $\Delta(\omega^2)$ is the difference between the squares of two consecutive eigenfrequencies of given orders n and n-1 (n = 2, 3, …). In Eq. (2b), **K** and **M** are

symmetric positive definite global stiffness and mass matrices (with corresponding element matrices available in [36]) of the generalized structural eigenvalue problem for the vibrating beam structure. Thus, the J candidate eigenfrequencies ($J > n$) considered in the optimization problem will all be real and can be ordered as follows by magnitude:

$$0 < \omega_1 \le \omega_2 \le \ldots \le \omega_J \tag{3}$$

Eq. (2c) imposes the conditions of $\mathbf{M}$ orthonormalization of the corresponding eigenvectors, where δ_{jk} denotes Kronecker's delta.

The dimensionless optimization problem (2) is discretized by subdividing the beam into N_E finite elements of equal lengths $l_e = 1/N_E$ with individual cross-sectional areas $\alpha_e \left(e = 1, \ldots, N_E\right)$, which play the role as design variables of the discretized problem. Hence, Eq. (2d) expresses the non-dimensional (unit) volume constraint for the problem, and in Eq. (2e) a positive minimum cross-sectional area constraint value $\alpha_{\min}$ is prescribed for the design variables $\alpha_e \left(e = 1, \ldots, N_E\right)$. The value of $\alpha_{\min}$ is to be chosen less than the mean (unit) value of the cross-sectional area of the dimensionless beam, and larger than zero to avoid singularity of the stiffness matrix.

Using an extended bound formulation, cf. [37,38,12], the original optimization problem in Eq. (2) can be reformulated as in Eq. (4) where two scalar variables β_1 and β_2 are introduced. These scalar variables denote the upper and lower bound parameters in the constraint equations (4b) and (4c), respectively, and at the same time the difference between them in the objective function will be maximized.

$$\begin{aligned}
&\max_{\beta_1, \beta_2, \alpha_1, \ldots, \alpha_{N_E}} \left\{\beta_2 - \beta_1\right\} && (a)\\
&\text{subject to} \\
&\beta_2 - \omega_j^2 \le 0, \; j = n, n+1, \ldots, J, && (b)\\
&\omega_j^2 - \beta_1 \le 0, \; j = 1, \ldots, n-1, && (c)\\
&\mathbf{K}\boldsymbol{\phi}_j = \omega_j^2 \mathbf{M}\boldsymbol{\phi}_j, \; j = 1, \ldots, J, && (d)\\
&\boldsymbol{\phi}_j^T \mathbf{M}\boldsymbol{\phi}_k = \delta_{jk}, \; j, k = 1, \ldots, J, && (e)\\
&\sum_{e=1}^{N_E} \alpha_e l_e - 1 \le 0, && (f)\\
&0 < \alpha_{\min} \le \alpha_e, \; e = 1, \ldots, N_E. && (g)
\end{aligned} \tag{4}$$

It is emphasized that the two bound variables β_1 and β_2 serve as design variables together with the cross-sectional areas. The bound formulation is convenient for handling of difficulties concerning multiple eigenfrequencies. To accommodate the possibility of existence or creation of multiple eigenfrequencies, sensitivity results for multiple eigenfrequencies are needed (see, e.g., [15,39] for an overview and papers cited therein), and the results will be briefly presented in the next section.

3 INCREMENTAL FORMULATION BASED ON SENSITIVITY RESULTS FOR SIMPLE AND MULTIPLE EIGENFREQUENCIES

The following brief account lends itself to Refs. [15,16].

3.1 Sensitivity results for simple eigenfrequencies

If the *j*-th eigenfrequency is simple (unimodal), the corresponding eigenvector $\boldsymbol{\phi}_j$ is unique (up to a multiplying factor) and the eigenfrequency will be differentiable with respect to the design variables α_e. The derivative of the *j*-th eigenvalue $\lambda_j = \omega_j^2$ with respect to a design variable α_e is given in [40],

$$\frac{\partial \lambda_j}{\partial \alpha_e} = \boldsymbol{\phi}_j^{\,T} \left(\frac{\partial \mathbf{K}}{\partial \alpha_e} - \lambda_j \frac{\partial \mathbf{M}}{\partial \alpha_e} \right) \boldsymbol{\phi}_j, \; e = 1, \ldots, N_E \,. \tag{5}$$

Here the derivatives of the dimensionless, global matrices **K** and **M** can be calculated explicitly from the element stiffness and mass matrices in [36]. If all the design variables are changed simultaneously, the linear increment $\Delta\lambda_j$ of the simple eigenvalue $\lambda_j = \omega_j^2$ is given by the scalar product

$$\Delta\lambda_j = \nabla\lambda_j^T \, \Delta\boldsymbol{\alpha} \,, \tag{6}$$

where $\Delta\boldsymbol{\alpha} = \left\{ \Delta\alpha_1, \cdots, \Delta\alpha_{N_E} \right\}^T$ is the vector of changes of the design variables $\alpha_e \left(e = 1, \ldots, N_E \right)$ and

$$\nabla\lambda_j = \left\{ \boldsymbol{\phi}_j^T \left(\frac{\partial \mathbf{K}}{\partial \alpha_1} - \lambda_j \frac{\partial \mathbf{M}}{\partial \alpha_1} \right) \boldsymbol{\phi}_j \,, \cdots\cdots, \boldsymbol{\phi}_j^T \left(\frac{\partial \mathbf{K}}{\partial \alpha_{N_E}} - \lambda_j \frac{\partial \mathbf{M}}{\partial \alpha_{N_E}} \right) \boldsymbol{\phi}_j \right\}^T \,, \tag{7}$$

is the vector of sensitivities (or gradients) of the eigenvalue λ_j with respect to the design variables.

3.2 Sensitivity results for multiple eigenfrequencies

If eigenfrequencies are multiple, they are not differentiable with respect to design variables in the usual sense. The difficulty is that any linear combination of the eigenvectors corresponding to a multiple eigenfrequency will satisfy the generalized eigenvalue problem (2b) and (4d), which implies that the eigenvectors are not unique. Hence, Eqs. (5)-(7) are not valid for multiple eigenfrequencies, and the derivation of design sensitivities of such eigenvalues is much more cumbersome, see, e.g. [15,16,39,41].

Our interest in multiple eigenfrequencies in the present context is due to the possibility that, as accounted for by the bound technique in Eqs. (4a-c), the upper eigenfrequency ω_n and lower eigenfrequency ω_{n-1} of the gap $\omega_n - \omega_{n-1}$ may be increased and decreased, respectively, to such an extent that one or both of them become multiple.

Thus, let us assume that the solution to the generalized, *M*-orthonormalized eigenvalue problem, Eqs. (2b,c) and Eqs. (4d,e) included in the optimization problems (2) and (4), yields a *N*-fold multiple eigenfrequency as the *upper* eigenfrequency of the gap to be maximized. The corresponding eigenvalue $\tilde{\lambda}$,

$$\tilde{\lambda} = \lambda_j = \omega_j^2, \quad j = n, \cdots, n+N-1 \tag{8}$$

will then be associated with the N ($N > 1$) eigenfrequencies ω_j with the lowest subscripts j appearing in the bound constraint (4b) in terms of β_2 which will be active for each of the above values of $j = n, \ldots, n+N-1$. In Eqs. (4) and (8) we shall assume $n+N-1 < J$, i.e., that the total number J of eigenfrequencies (counted with multiplicity) considered in problem (4) is chosen such that the J-th eigenfrequency ω_J is larger than the multiple eigenfrequency corresponding to $\tilde{\lambda}$ in Eq. (8).

Analogously, the orthonormalized eigenvalue problem (2b,c) and (4d,e) contained in problems (2) and (4) may yield an R-fold multiple eigenfrequency as the *lower* eigenfrequency of the gap. The corresponding eigenvalue $\hat{\lambda}$,

$$\hat{\lambda} = \lambda_j = \omega_j^2, \; j = n-R, \cdots, n-1, \tag{9}$$

is then associated with the R ($R>1$) eigenfrequencies ω_j with the largest subscripts j included in the bound constraint (4c) in terms of β_1 which will be active for each of the values of $j = n-R, \ldots, n-1$ in Eq. (9). In this case we shall assume that $1 \le n-R$.

Now, following [15,16,39] one finds that both for the upper (possibly N-fold) and lower (possibly R-fold) eigenfrequency of the gap, the increments $\Delta\lambda_j = \Delta(\omega_j^2)$ of the N and R members λ_j of the multiple eigenvalue $\tilde{\lambda}$ in Eq. (8) and $\hat{\lambda}$ in Eq. (9), respectively, are given by the N- respectively R-dimensional algebraic sub-eigenvalue problem

$$\det\left[\mathbf{f}_{sk}^T \Delta\boldsymbol{\alpha} - \delta_{sk}\Delta(\omega^2)\right] = 0, \tag{10}$$

where δ_{sk} is Kronecker's delta, and $\mathbf{f}_{sk}$ denote generalized gradient vectors of the form

$$\mathbf{f}_{sk}^T = \left\{ \boldsymbol{\phi}_s^T \left(\frac{\partial \mathbf{K}}{\partial \alpha_1} - \lambda_j \frac{\partial \mathbf{M}}{\partial \alpha_1} \right) \boldsymbol{\phi}_k, \ldots, \boldsymbol{\phi}_s^T \left(\frac{\partial \mathbf{K}}{\partial \alpha_{N_E}} - \lambda_j \frac{\partial \mathbf{M}}{\partial \alpha_{N_E}} \right) \boldsymbol{\phi}_k \right\}. \tag{11}$$

Note that both in Eqs. (10) and (11), $s,k = n, \ldots, n+N-1$ relate to a N-fold upper eigenfrequency of the gap, cf. Eq. (8), and $s,k = n-R, \ldots, n-1$ pertain to an R-fold lower eigenfrequency of the gap, see Eq. (9).

According to the definition in Eq. (11), each $\mathbf{f}_{sk}$ is a N_E-dimensional vector, and $\mathbf{f}_{sk}^T \Delta\boldsymbol{\alpha}$ in Eq. (10) is a scalar product for each $s,k = n, \ldots, n+N-1$ in the N-dimensional, and each $s,k = n-R, \ldots, n-1$ in the R-dimensional, matrix in Eq. (10). The label 'generalized gradient vector' for $\mathbf{f}_{sk}$ becomes apparent when comparing Eq. (11) with the expression for the gradient vector $\nabla\lambda_j$ of a simple eigenvalue λ_j in Eq. (7). Note also that $\mathbf{f}_{sk} = \mathbf{f}_{ks}$ due to the symmetry of the matrices $\mathbf{K}$ and $\mathbf{M}$, and that the two subscripts s and k refer to the orthonormalized eigenvectors from which $\mathbf{f}_{sk}$ is calculated.

As one may expect, for $N = 1$, i.e., $j = s = k = n$, Eqs. (8) and (10) verify that the upper eigenfrequency of the gap corresponds to the simple (unimodal) eigenvalue $\lambda_n = \omega_n^2$. In this case, Eq. (10) reduces to the simple algebraic equation

$$\mathbf{f}_{nn}^T \Delta\boldsymbol{\alpha} - \Delta\lambda_n = 0, \tag{12}$$

where, according to Eqs. (6), (11) and (7), we have

$$\mathbf{f}_{nn} = \nabla \lambda_n \,, \tag{13}$$

i.e., $\mathbf{f}_{nn}$ is simply the vector of sensitivities of the unimodal eigenvalue $\lambda_n = \omega_n^2$ with respect to the design variables α_e, e = 1, …, N_E, cf. Eqs. (5) and (7).

Analogously, for R=1, i.e., $j = s = k = n - 1$, Eqs. (9) and (10) verify that the lower eigenfrequency of the gap corresponds to the simple eigenvalue $\lambda_{n-1} = \omega_{n-1}^2$.

These observations have the important implication that the computational procedure delineated in the sequential sub-section is applicable independently of whether the upper and/or lower eigenfrequencies that define the gap, are members of a multiple eigenfrequency or are just a simple eigenfrequency.

3.3 Incremental formulation of the optimization problem

Based on the sensitivity analysis results in Sub-sections 3.1 and 3.2, the bound formulation of the optimization problem in Eq. (4) can be written in the following incremental form:

$$\max_{\beta_1, \beta_2, \Delta\alpha_1, \ldots, \Delta\alpha_{N_E}} \{\beta_2 - \beta_1\} \qquad (a)$$

subject to

$$\begin{aligned}
&\beta_2 - \left(\omega_j^2 + \mathbf{f}_{jj}^T \Delta\boldsymbol{\alpha}\right) \le 0,\ j = n + N = J, && (b)\\
&\beta_2 - \left[\omega_j^2 + \Delta\left(\omega_j^2\right)\right] \le 0,\ j = n, \ldots, n + N - 1, && (c)\\
&\left[\omega_j^2 + \Delta\left(\omega_j^2\right)\right] - \beta_1 \le 0,\ j = n - R, \ldots, n - 1,\ (n - R \ge 1), && (d)\\
&\left(\omega_j^2 + \mathbf{f}_{jj}^T \Delta\boldsymbol{\alpha}\right) - \beta_1 \le 0,\ j = n - R - 1,\ (if\ n - R \ge 2), && (e)\\
&\det\left[\mathbf{f}_{sk}^T \Delta\boldsymbol{\alpha} - \delta_{sk} \Delta\left(\omega^2\right)\right] = 0,\ s, k = n, \ldots, n + N - 1, && (f)\\
&\det\left[\mathbf{f}_{sk}^T \Delta\boldsymbol{\alpha} - \delta_{sk} \Delta\left(\omega^2\right)\right] = 0,\ s, k = n - R, \ldots, n - 1, && (g)\\
&\mathbf{K}\boldsymbol{\phi}_j = \omega_j^2 \mathbf{M}\boldsymbol{\phi}_j,\ j = 1, \ldots, J, && (h)\\
&\boldsymbol{\phi}_j^T \mathbf{M}\boldsymbol{\phi}_k = \delta_{jk},\ j, k = 1, \ldots, J, && (i)\\
&\sum_{e=1}^{N_E} \left(\alpha_e + \Delta\alpha_e\right) l_e - 1 \le 0, && (j)\\
&0 < \alpha_{\min} \le \alpha_e + \Delta\alpha_e,\ e = 1, \ldots, N_E. && (k)
\end{aligned} \tag{14}$$

Referring to the algebraic sub-eigenvalue problem in Eq. (10), the solutions of Eqs. (14f,g) correspond to the increments of the upper (possibly N-fold) and lower (possibly R-fold) eigenfrequency of the gap, respectively. These increments $\Delta(\omega_j^2)$ will enter respectively the upper and lower bound constraints Eqs. (14c,d) for the incremented multiple eigenfrequencies. In fact, Eqs. (14f,g) establish a relation between the independent variable increment vector $\Delta\boldsymbol{\alpha}$ and the dependent variables $\Delta(\omega_j^2)$. The incremental formulation in Eq. (14) solves a sub-optimization problem that furnishes optimum values of increments of the design variables. Then, the design variables are updated by iterative addition of the increments obtained until convergence, see [15] with a publisher's erratum [16] for further

details on this two-loop iterative procedure.

With the sensitivity results, the sub-optimization problem in Eq. (14) can be solved by using a mathematical programming method, e.g., MMA (see Ref. [42]). Alternatively, instead of the constraints in Eqs. (14f,g), $N\left(N-1\right)/2$ and $R\left(R-1\right)/2$ constraints $\mathbf{f}_{sk}^{T}\Delta\boldsymbol{\alpha}=0,\ s\neq k$, respectively, may be introduced for the β_2- and β_1-bound constraints, such that it is possible to compute the linear increments of both simple and multiple eigenvalues by the same, simple expression

$$\Delta\left(\omega_j^2\right)=\mathbf{f}_{jj}^{T}\Delta\boldsymbol{\alpha}, \tag{15}$$

where $j=n,\ldots,n+N-1$ for active β_2-bound constraints, and $j=n-R,\ldots,n-1$ for active β_1-bound constraints. In the present paper, the approach of introducing the constraints $\mathbf{f}_{sk}^{T}\Delta\boldsymbol{\alpha}=0,\ s\neq k$ is used for solving the sub-optimization problem. Further details of this approach are available in [43].

As mentioned in the end of the preceding sub-section, the formulation in Eq. (14) is applicable for problems with any mix of multiple and simple eigenfrequencies. Notice that if *N* and *R* are equal to unity, Eqs. (14f,g) reduce to the pertinent single algebraic equation for the increment of a simple eigenfrequency.

4 NUMERICAL EXAMPLES

4.1 Cantilever beams

Here, examples of cantilever beam designs for maximized higher order natural frequency (eigenfrequency) gaps $\Delta\omega_3=\left(\omega_3-\omega_2\right)$, $\Delta\omega_4=\left(\omega_4-\omega_3\right)$, $\Delta\omega_9=\left(\omega_9-\omega_8\right)$, $\Delta\omega_{10}=\left(\omega_{10}-\omega_9\right)$, $\Delta\omega_{19}=\left(\omega_{19}-\omega_{18}\right)$ and $\Delta\omega_{20}=\left(\omega_{20}-\omega_{19}\right)$ will be presented. For reasons of accuracy, an initial finite element study was carried out to ensure that calculated natural frequencies were convergent with respect to the number of elements applied along the length of the beam. Based on this study, 200 elements were adopted for the first two beam designs, and 1000 elements for the last four designs where relatively higher order natural frequencies are considered. The optimized beam designs are shown in Figs. 1, 2, 3(b), 4(d), 6(b) and 7(b). Each of these and subsequent designs in this paper are illustrated to suitable scale by their shape (contour) curves $\pm\sqrt{\alpha\left(x\right)}$, $0\le x\le 1$, after calculation of their linear dimensions $\pm\sqrt{\alpha_e}$ perpendicular to the beam axis. A lower limit $\alpha_{\min}$=0.05 is prescribed for the non-dimensional cross-sectional area in all the examples presented in the present and the two sequential sub-sections.

In order to have a convenient reference for evaluation and discussion of the optimization results, we choose a non-dimensional comparison beam with uniform cross-section and the same material, boundary conditions, (unit) volume, (unit) length, and cross-section parameter *c* as the optimized non-dimensional beams. The gap between the *n*-th and (*n-1*)-th natural frequencies of this uniform beam is denoted as $\Delta\omega_n^u$, and for the frequency gaps to be considered here, we find that $\Delta\omega_3^u$ =39.66, $\Delta\omega_4^u$ =59.20, $\Delta\omega_9^u$ =157.91, $\Delta\omega_{10}^u$ =177.65, $\Delta\omega_{19}^u$ =355.31, and $\Delta\omega_{20}^u$ = 375.04.

The corresponding frequency gaps obtained by optimization are significantly larger. Thus, the optimized cantilever beam designs in Figs. 1, 2, 3(b), 4(d), 6(b) and 7(b) have the

following frequency gaps, $\Delta\omega_3$ =129.72, $\Delta\omega_4$ =195.15, $\Delta\omega_9$ =1144.81, $\Delta\omega_{10}$ =1332.25, $\Delta\omega_{19}$ = 5141.39 and $\Delta\omega_{20}$ = 5542.40.

The designs optimized for maximum frequency gaps $\Delta\omega_3$ and $\Delta\omega_4$ subject to $\alpha_{\min}$ =0.05 in Figs. 1 and 2, respectively, are almost indistinguishable from optimum designs obtained and illustrated in Ref. [24] for the similar problems of maximizing the higher order natural frequencies ω_3 and ω_4 without a minimum constraint for the cross-sectional area of the beams; compare Figs. 1 and 2 in the present paper with Figs. 5 and 6 in [24], where the latter type of problem is treated. The designs in Figs. 1 and 2 are both obtained by using the uniform comparison beam as an unbiased initial design.

As a matter of fact, the number of local optimum designs increases with increasing values of the orders *n* and *n*-1 of the eigenfrequencies that define the frequency gap to be maximized, and with the small lower limit $\alpha_{\min}$ =0.05 prescribed for the cross-sectional area in the current examples, it turned out that for values of $n > 4$, possible optimum designs could no longer be obtained by using the uniform comparison beam as an initial design for the iterative computational procedure. Now, in order to obtain presumed optimum designs maximizing the frequency gap $\Delta\omega_n$, for given values of $n > 4$, we assumed – as was found for the cases of maximizing the frequency gaps $\Delta\omega_3$ and $\Delta\omega_4$ described above – that the design subject to the minimum allowable cross-sectional area $\alpha_{\min}$ =0.05 would be very similar to the design solution to the problem of maximizing the higher order natural frequency ω_n without specification of a minimum cross-sectional area constraint (which, in the current context, corresponds to setting $\alpha_{\min}$ =0). As already indicated in the Introduction, the latter type of problem is quite extensively covered in Ref. [24], and in Section 5 of the present paper it is briefly described how the "Method of Scaled Optimum Beam Elements" developed in [24] may be used to determine the design of a vibrating cantilever beam that maximizes an eigenfrequency of given, higher order when $\alpha_{\min}$ =0.

We shall now present examples of optimizing cantilever beam designs for maximum values of the natural frequency gaps $\Delta\omega_9$, $\Delta\omega_{10}$, $\Delta\omega_{19}$ and $\Delta\omega_{20}$ subject to the minimum cross-sectional area constraint value $\alpha_{\min}$ =0.05, i.e., examples where the possible optimum beam designs could not be obtained by applying the uniform comparison beam as an initial design in the iterative computational procedure presented in this paper.

Thus, in order to obtain the presumed optimum design maximizing the frequency gap $\Delta\omega_9$ subject to $\alpha_{\min}$ =0.05, shown in Fig. 3(b), we applied a *biased* initial design which was very similar to the optimized design obtained by application of the "Method of Scaled Optimum Beam Elements" [24] as described in Section 5 by way of the example of maximizing the 9-th natural frequency of a transversely vibrating cantilever with inner points of zero cross-sectional area and beam separation (due to $\alpha_{\min}$ =0). The design obtained by this approach was only modified by changing the cross-sectional area to be nowhere less than the value of $\alpha_{\min}$, i.e., $\alpha_{\min}$ =0.05, before it was applied as a biased initial design for the maximization of $\Delta\omega_9$ subject to this constraint value.

The resulting optimized design in Fig. 3(b) distinctly exhibits periodicity. The two natural frequencies defining the gap $\Delta\omega_9$ are both unimodal, but very close to neighbouring frequencies. The maximized frequency gap $\Delta\omega_9$ of the design, cf. the caption of Fig. 3(b), is

found to be substantially larger than the corresponding frequency gap obtained when using the uniform comparison beam as an initial design for the optimization. This may indicate that the design in Fig. 3(b) is the "best" optimum solution to the problem considered. Fig. 3(a) shows to suitable scale the free vibration modes $\phi_9(x)$ and $\phi_8(x)$ corresponding to the normalized and mutually orthogonal mode shape vectors $\boldsymbol{\phi}_9$ and $\boldsymbol{\phi}_8$ associated with the eigenfrequencies ω_9 and ω_8 that define the maximized frequency gap $\Delta\omega_9 = (\omega_9 - \omega_8)$ of the presumed optimum design in Fig. 3(b).

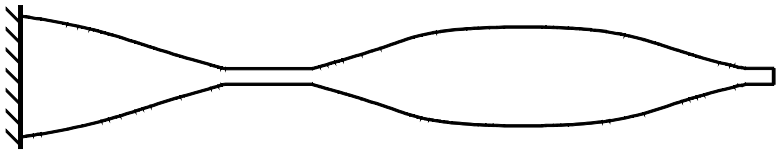

Figure 1: Cantilever with maximized frequency gap $\Delta\omega_3$ = 129.72. $\Delta\omega_3^u$ =39.66 for the comparison design

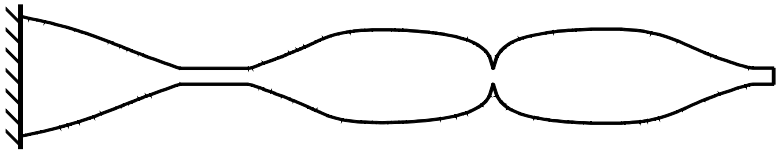

Figure 2: Cantilever with maximized frequency gap $\Delta\omega_4$ =195.15. $\Delta\omega_4^u$ =59.20 for the comparison design

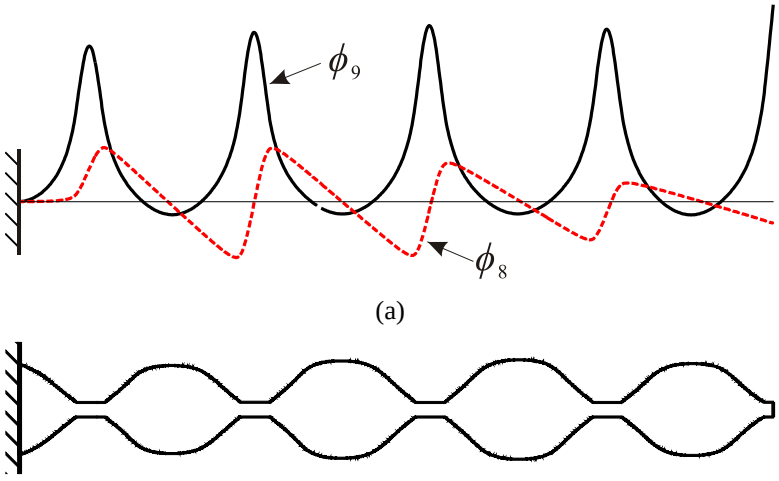

Figure 3: Cantilever with maximized frequency gap $\Delta\omega_9$ =1144.81. $\Delta\omega_9^u$ =157.91 for the comparison design. (a) Mode shapes, (b) Optimized design

With a view to obtain a physical understanding of the frequency gap mechanism, we take a closer look at the variations of the vibration modes $\phi_9(x)$, $\phi_8(x)$ and beam shape $\pm\sqrt{\alpha(x)}$ along the length $0 \le x \le 1$ of the optimized dimensionless beam in Fig. 3. Since $\phi_9(x)$ and $\phi_8(x)$ are normalized eigenfunctions associated with the eigenfrequencies ω_9 and ω_8 for the beam with the cross-sectional area function $\alpha(x)$, then, according to Rayleigh's

principle, the two eigenfrequencies are given by

$$\omega_i^2 = \int_0^1 \alpha^2 \left(\phi_i''\right)^2 dx\,,\ i = 8, 9\,. \tag{16}$$

In this equation, the integral is proportional to the elastic bending energy corresponding to the mode $\phi_i(x)$.

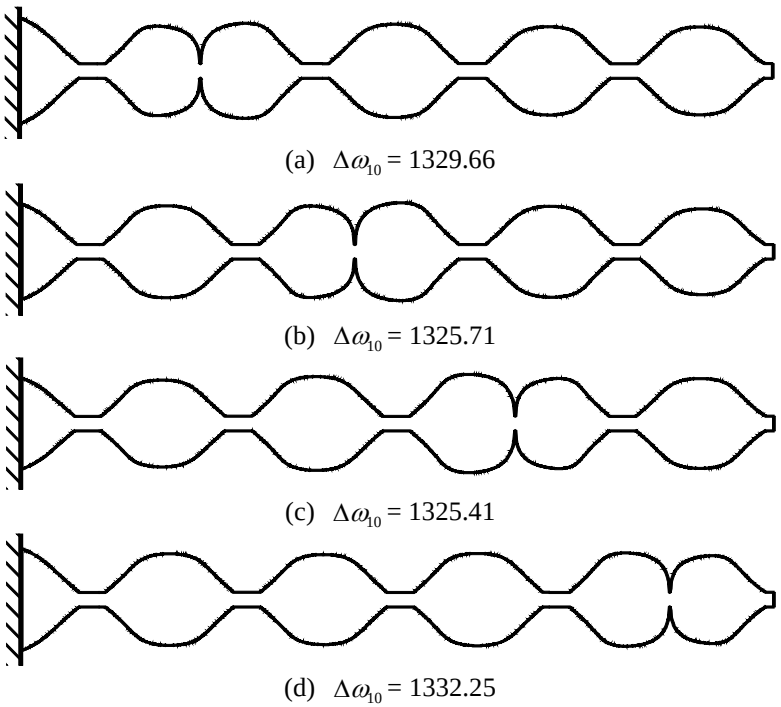

(a) $\Delta\omega_{10}$ = 1329.66

(b) $\Delta\omega_{10}$ = 1325.71

(c) $\Delta\omega_{10}$ = 1325.41

(d) $\Delta\omega_{10}$ = 1332.25

Figure 4: Cantilevers with maximized frequency gaps $\Delta\omega_{10}$. $\Delta\omega_{10}^{u}$ =177.65 for the comparison design. (a), (b) and (c) Local optimum solutions. (d) Presumed global optimum solution

Figure 5: Local optimum cantilever associated with frequency gap $\Delta\omega_{10}$ =901.09

The physical mechanism behind the maximized gap between the natural frequencies ω_9 and ω_8 is as follows. When vibrating with the mode ϕ_9, see Fig. 3(a), a large value of the associated frequency ω_9 is obtained by absorption of large elastic bending energy in the segments with the larger, non-uniform cross-sectional areas, cf. Eq. (16), whereas negligible bending energy is absorbed in the small, uniform segments with high flexibility. When the beam vibrates with the mode ϕ_8, see Fig. 3(a), the associated frequency ω_8 becomes very small (and the frequencies of lower order even smaller) because only the beam segment adjacent to the clamped beam end receives a small amount of bending energy. However, the nota-

ble feature is that each of the other segments of the beam essentially perform rigid body motions in a piecewise linear mode without bending, and therefore support a low value of ω_8. The bending energy from the curvatures of the "kinks" of mode ϕ_8 is negligible in Eq. (16) because the kinks occur in the small, uniform segments with high flexibility.

Figs. 4(a)-(d) depict four design solutions obtained for the problem of maximizing the natural frequency gap $\Delta\omega_{10}$. Although the values of the frequency gaps $\Delta\omega_{10}$ given for the designs in Fig. 4 are very close to each other, the four designs are seen to be distinctly different, and the eigenfrequencies defining the gaps $\Delta\omega_{10}$ are all found to be unimodal. Since the values of the frequency gaps $\Delta\omega_{10}$ are smaller for the designs in Figs. 4(a-c) than the value of the gap $\Delta\omega_{10}$ for the design in Fig. 4(d), the designs in Figs 4(a-c) must be considered to be local optimum designs, and we presume that the design in Fig. 4(d) is the global optimum design for the current problem. We managed to obtain the four different designs by applying a *biased* initial design for each of them that was very similar to one of four alternative, presumed global optimum designs available in [24] for the problem of maximizing the 10-th natural frequency when inner points of vanishing cross-sectional area are allowed.

Fig. 5 shows the design that resulted from applying the uniform comparison beam as an *unbiased* initial design when attempting to maximize the frequency gap $\Delta\omega_{10}$. As is seen from the caption of Fig. 5, the value of the frequency gap $\Delta\omega_{10}$ for this distinctly different design is much lower than that of the design in Fig. 4(d), so the design in Fig. 5 is only a local optimum solution.

Next, we present examples of cantilever beams with maximized gaps between adjacent frequencies of higher orders, i.e., $\Delta\omega_{19} = \left(\omega_{19} - \omega_{18}\right)$ and $\Delta\omega_{20} = \left(\omega_{20} - \omega_{19}\right)$. The optimized designs are shown in Figs. 6(b) and 7(b). Both beam designs are distinct, and the eigenfrequencies defining the maximized frequency gaps of the designs are both found to be unimodal, albeit very close to neighbouring eigenfrequencies.

Figs. 6(b) and 7(b) clearly show the important result that except for beam segments adjacent to the beam ends (whose designs are characteristic for the specific boundary conditions considered), the entire inner part of each of the optimum beam designs exhibit a *significant periodicity in terms of repeated beam segments of the same type*. By comparing the optimized designs in Figs. 6(b) and 3(b) and in Figs. 7(b) and 4(d), respectively, it may be concluded that the degree of this inner periodicity increases with increasing values of the orders *n* and *n-1* of the natural frequencies that define the frequency gap subjected to maximization. The free vibration modes ϕ_{19} and ϕ_{18} are drawn on the basis of the mode shape vectors $\boldsymbol{\phi}_{19}$ and $\boldsymbol{\phi}_{18}$ corresponding to the natural frequencies ω_{19} and ω_{18} that define the frequency gap $\Delta\omega_{19} = \left(\omega_{19} - \omega_{18}\right)$, and are shown in Fig. 6(a). Similarly, the free vibration modes ϕ_{20} and ϕ_{19} corresponding to the natural frequencies ω_{20} and ω_{19} defining the gap $\Delta\omega_{20} = \left(\omega_{20} - \omega_{19}\right)$ are shown in Fig. 7(a). Here, it is interesting to study the influence on the modes of the inner "dip" in the (new) beam segment at the free end of the design in Fig. 7(b). Note finally that it is obvious from Figs. 6 and 7 that the physical frequency gap mechanism described in connection with Fig. 3, also manifests itself in the current examples.

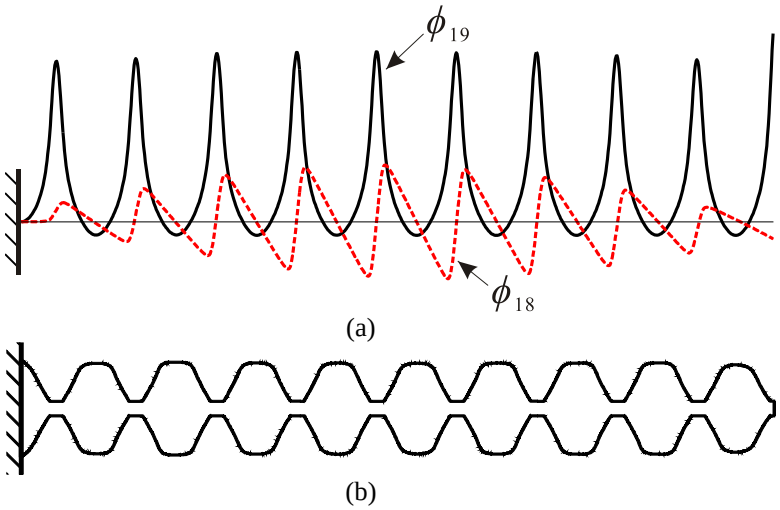

Figure 6: Cantilever with maximized frequency gap $\Delta\omega_{19}$ = 5141.39. $\Delta\omega_{19}^{u}$ =355.31 for the comparison design. (a) Mode shapes, (b) Optimized design

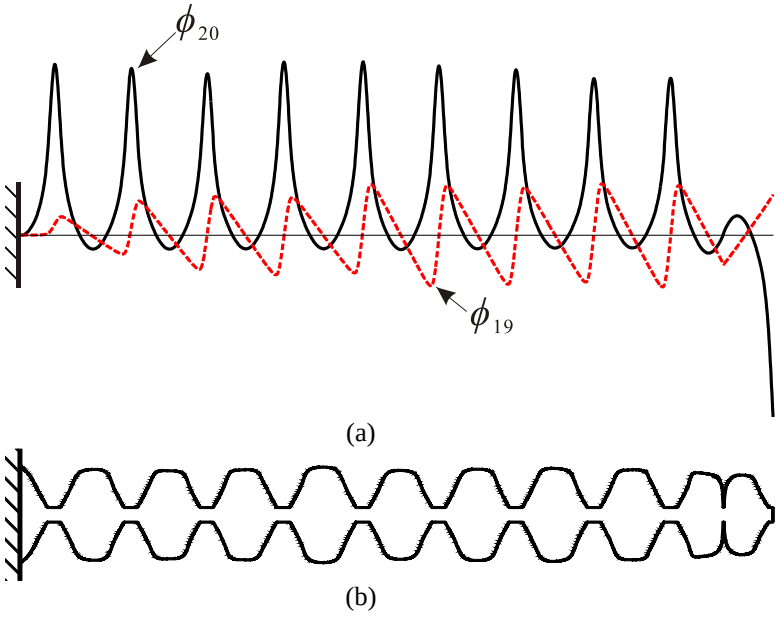

Figure 7: Cantilever with maximized frequency gap $\Delta\omega_{20}$ = 5542.40. $\Delta\omega_{20}^{u}$ =375.04 for the comparison design. (a) Mode shapes, (b) Optimized design

4.2 Clamped-clamped beams

Here, we present a few examples of optimizing clamped-clamped Bernoulli-Euler beams, still assuming a lower limit $\alpha_{\min}$ =0.05 to be prescribed for the non-dimensional cross-sectional area of the beams. The frequency gaps considered are $\Delta\omega_4$, $\Delta\omega_9$ and $\Delta\omega_{10}$, and their maximized values are found to be $\Delta\omega_4$ =309.74, $\Delta\omega_9$ =1411.34 and $\Delta\omega_{10}$ =1617.91,

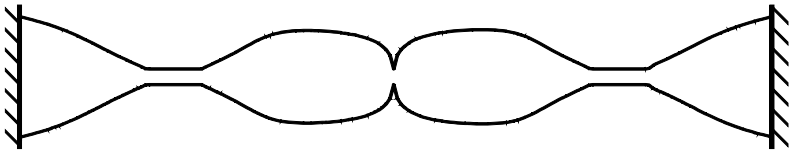

Figure 8: Clamped-clamped beam with maximized frequency gap $\Delta\omega_4$ =309.74. $\Delta\omega_4^u$ =78.96 for the comparison design

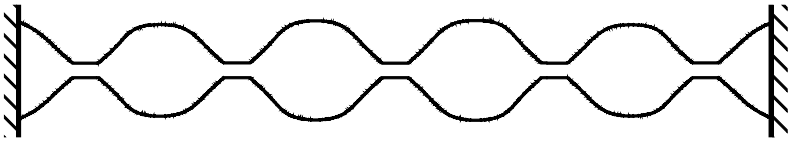

Figure 9: Clamped-clamped beam with maximized frequency gap $\Delta\omega_9$ =1411.34. $\Delta\omega_9^u$ =177.65 for the comparison design

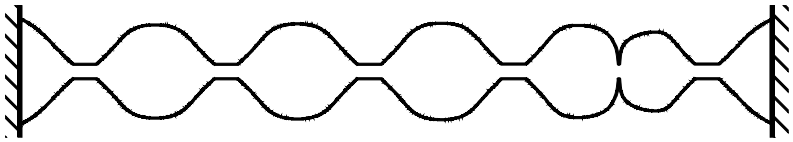

Figure 10: Clamped-clamped beam with maximized frequency gap $\Delta\omega_{10}$ =1617.91. $\Delta\omega_{10}^u$ =197.39 for the comparison design

which are significantly larger than the corresponding values $\Delta\omega_4^u$ =78.96, $\Delta\omega_9^u$ =177.65, and $\Delta\omega_{10}^u$ =197.39 for the uniform, clamped-clamped comparison beam.

The optimized beam designs are shown in Figs. 8, 9 and 10, and it is interesting to compare the design in Fig. 8 in the present paper with that in the bottom of Fig. 13 in Ref. [24]. We note that – as in Figs. 3(b) and 4(d) – it is seen in Figs. 9 and 10 that periodicity, i.e., repetition of segments of the same type, already appears in the inner part of the beam designs with maximized frequency gaps that correspond to relatively low orders of the respective natural frequencies. However, the segments adjacent to the beam ends are generally different due to different characteristics of the specific boundary conditions considered.

4.3 Clamped-simply supported beams

In this section, a few examples of Bernoulli-Euler beams clamped at one end and simply supported at the other end will be optimized. The same lower limit $\alpha_{\min}$ =0.05 as above is prescribed. The frequency gaps considered are $\Delta\omega_4$, $\Delta\omega_9$ and $\Delta\omega_{10}$, and their maximized values are found to be $\Delta\omega_4$ =274.72, $\Delta\omega_9$ =1226.18 and $\Delta\omega_{10}$ =1541.79, i.e., they are significantly larger than the corresponding values $\Delta\omega_4^u$ =74.02, $\Delta\omega_9^u$ =172.72, and $\Delta\omega_{10}^u$ = 192.46 for the uniform, clamped-simply supported comparison beam.

The optimized beam designs are shown in Figs. 11, 12 and 13. Periodicity can be observed in the inner part of the beam designs with maximized band-gaps $\Delta\omega_9$ and $\Delta\omega_{10}$, see Figs. 12 and 13. The segments adjacent to the simply supported end are generally different from those adjacent to the free or clamped end. Two different kinds of segments adjacent to the simple end support are seen in Figs. 12 and 13 that depict the beams maximizing the frequency gaps $\Delta\omega_9$ and $\Delta\omega_{10}$, respectively. This point will be discussed in Section 5.

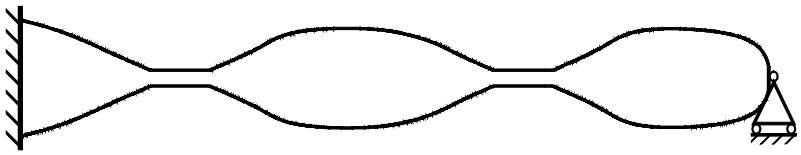

Figure 11: Clamped-simply supported beam with maximized frequency gap $\Delta\omega_4$ =274.72. $\Delta\omega_4^u$ =74.02 for the comparison design

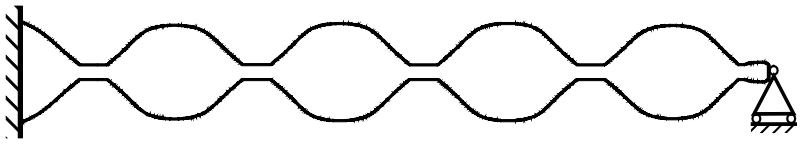

Figure 12: Clamped-simply supported beam with maximized frequency gap $\Delta\omega_9$ =1226.18. $\Delta\omega_9^u$ = 172.72 for the comparison design

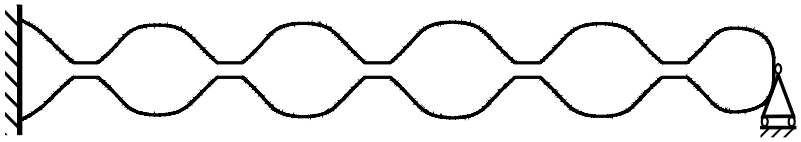

Figure 13: Clamped-simply supported beam with maximized frequency gap $\Delta\omega_{10}$ = 1541.79. $\Delta\omega_{10}^u$ = 192.46 for the comparison design

4.4 Optimum design with larger minimum area constraint value

Figs. 14, 15 and 16 depict the designs obtained by maximizing the frequency gap $\Delta\omega_9$ of a cantilever, a clamped-clamped, and a clamped-simply supported Bernoulli-Euler beam when applying a larger cross-sectional area constraint value, namely $\alpha_{\min}$ =0.5. The values of the frequency gaps $\Delta\omega_9$ for the optimized beams and the gaps $\Delta\omega_9^u$ for the corresponding uniform comparison beams are given in the captions of Figs. 14, 15 and 16.

When comparing the optimized beams in Figs. 14, 15 and 16 with the corresponding ones (same order of frequency gap and same boundary conditions) in Figs. 3(b), 9 and 12, respectively, we make the important observation that pronounced repetitions of similar segments are found in the inner parts of all these beams, and that the same degrees of periodicity in the beams in Figs. 3, 9 and 12 are obtained in the beams in Figs. 14, 15 and 16, although the latter are optimized with the considerably larger value $\alpha_{\min}$ =0.5 of the minimum cross-sectional area constraint.

By the comparison of the above-mentioned figures, we also verify that due to their larger design freedom, the beams optimized with the small value $\alpha_{\min}$ =0.05 of the lower cross-sectional area limit, are associated with significantly larger increases of the maximized frequency gaps.

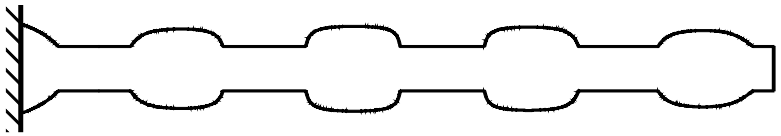

Figure 14: Cantilever with maximized frequency gap $\Delta\omega_9$ =377.91 subject to a minimum cross-sectional area constraint value 0.5. $\Delta\omega_9^u$ =157.91 for the comparison design

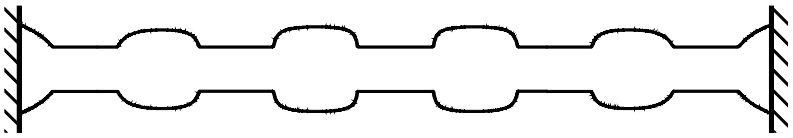

Figure 15: Clamped-clamped beam with maximized frequency gap $\Delta\omega_9$ =460.64 subject to a minimum cross-sectional area constraint value 0.5. $\Delta\omega_9^u$ =177.65 for the comparison design

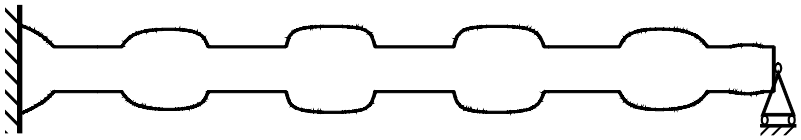

Figure 16: Clamped-simply supported beam with maximized frequency gap $\Delta\omega_9$ = 431.06 subject to a minimum cross-sectional area constraint value 0.5. $\Delta\omega_9^u$ = 172.72 for the comparison design

5 DISCUSSION

Up to now, we have considered optimum design of Bernoulli-Euler beams with the objective of maximizing, for a specified value of *n*, the separation (gap) between the (higher-order) *n*-th and (*n*-1)-th eigenfrequencies, subject to a prescribed positive value of a non-dimensional minimum allowable cross-sectional area $\alpha_{\min}$ which has been chosen as $\alpha_{\min}$ =0.05 in Sub-sections 4.1, 4.2 and 4.3, and $\alpha_{\min}$ =0.5 in Sub-section 4.4.

In this section, we shall briefly discuss the characteristics of this eigenfrequency gap optimization problem in the limiting case where the cross-sectional area function is geometrically unconstrained (except for the given volume). This means that no minimum constraint is specified for the cross-sectional area of the beam, i.e., the cross-sectional area is allowed to attain zero value in discrete points on the beam axis. *In this special case (that corresponds to* $\alpha_{\min} = 0$ *in the context of this paper), the solutions to our problem of maximizing the gap between the eigenfrequencies* ω_n *and* ω_{n-1} *are the same as the solutions to the problem of maximizing a single, higher order eigenfrequency* ω_n *of given order n for specified volume, length, and boundary conditions of the beam*. The latter problem is treated in Ref. [24], where a large number of optimum designs are available.

The reason why the two different beam optimization problems have identical solutions, may be explained as follows. When a single eigenfrequency ω_n of given higher order *n* is maximized without specification of a minimum constraint on the cross-sectional area, the optimized beam turns out to possess *n*-1 degrees of kinematic freedom to perform rigid motions, since the cross-section vanishes at inner singular points of the beam. At these points, either *inner hinges* of zero bending moment and finite shear force, or, predominantly, *inner separations* with both zero bending moment and zero shear force, are created by the optimization of the *n*-th eigenfrequency. This has the effect that simultaneously with the

maximization of the *n*-th eigenfrequency, the *n*-1 degrees of kinematic freedom of the beam turn all the *n*-1 modes associated with the lower order eigenfrequencies into rigid body motions, and all these frequencies (including that of order *n*-1) are therefore equal to zero.

Thus, besides maximizing the *n*-th eigenfrequency of the beam, the problem formulation in Ref. [24] covers the current problem of maximizing the difference (gap) between the *n*-th and the (*n*-1)-th eigenfrequencies of the beam, if $\alpha_{\min} = 0$.

The optimized beams associated with the small minimum cross-sectional area constraint value $\alpha_{\min}$ =0.05 in Sub-sections 4.1, 4.2, and 4.3 strongly indicate the locations of formation of inner hinges and inner separations in the limiting case of $\alpha_{\min} = 0$. In Fig. 1, for example, the comparatively large inner beam segment with active minimum cross-sectional area constraint will shrink to a single point with the formation of an inner separation between the two parts of the beam in the limiting case of $\alpha_{\min} = 0$. In Fig. 2, the narrow "dip" in the cross-sectional area function indicates a point where an inner hinge with zero bending moment will be created in the case of $\alpha_{\min} = 0$. A large number of similar points with formation of inner beam separations and hinges in the case of $\alpha_{\min} = 0$ are easily identified in the figures. It is worth noting that in each of the optimum designs shown, there is no more than a single inner point with a narrow "dip" in the area function indicating formation of an inner hinge in the case of $\alpha_{\min} = 0$, but an increasing number of points that indicates creation of inner separations, when the given order of the frequency gap is increased. An exception is the design in Fig. 5 which contains several narrow "dips", but this is a *local, and not global optimum solution*.

In the optimum designs with one end clamped and the other end simply supported, see Figs. 12 and 13, we observe two kinds of segments adjacent to the simply supported end. Quite surprisingly, for the design shown in Fig. 12, the beam segment at the simply supported end will shrink to a separation in the limiting case of $\alpha_{\min} = 0$, where both the bending moment and shear force are zero at the end point of the beam. Hence, as is discussed in [24], the beam disconnects from the support, i.e., the separation makes the simple support superfluous. This implies that the optimum solution in the limiting the case of $\alpha_{\min} = 0$ will be the same as that with a free end instead of the original simply supported end. Contrary to this, the beam segment adjacent to the simply supported end in Fig. 13 will not shrink to a separation in the limiting case of $\alpha_{\min} = 0$, but remain connected to the hinge at the end point. Thus, in this case, the optimum solution behaves as expected and takes advantage of the simple support.

In Ref. [24], the dimensionless beam optimization problem is first solved for small values of *n* for various combinations of classical boundary conditions. This is done by successive iterations based on a numerical integration of the governing equations, where singularities in the *n*-th eigenmode and its derivatives are isolated at points of zero beam cross-sectional area for reasons of accuracy and convergence. Hereby a small number of different types of optimally designed, non-dimensional beam elements are produced. By proper scaling, these beam elements can be used as building blocks for optimum beams associated with much larger values of the prescribed order of their *n*-th eigenfrequency.

Since, as mentioned above, at most one inner hinge will appear in a global optimum beam with $\alpha_{\min} = 0$, and an inner hinge can be included in optimized non-dimensional beam elements mentioned above, then all other inner points of vanishing cross-sectional area in an optimum beam associated with a sufficiently large value of *n*, will be inner separations

between optimized beam elements. This is very important because the inner separations provide the means to solve very easily the optimization problem for a sufficiently large value of *n* by an optimum scaling of the optimized non-dimensional beam elements by means of very simple analytical formulas derived in [24].

As an example, let us consider the approach of determining the design of a vibrating cantilever beam that maximizes, say, the 9-th eigenfrequency ω_9 and hence the frequency gap $\Delta\omega_9 = \left(\omega_9 - \omega_8\right)$ of the beam with $\alpha_{\min}$=0. (Note that the optimized beam with $\alpha_{\min}$ = 0.05 is shown in Fig. 3.) The first step of the method consists in applying Table 2 and Eq. (30) in Ref. [24] which easily yields that the optimum cantilever design associated with *n*=9 will have four inner separations and be composed of (or assembled as) five dimensionless, optimized elements (or segments) along the length of the beam: an element "a" consisting of a cantilever optimized for *n*=1 (see Fig. 1 in Ref. [24]), followed by four elements "c" (see Fig. 11 in the reference), each consisting of a free-free beam optimized for *n*=3 (the order of the lowest non-vanishing eigenfrequency for such a beam). The four (identical) "c" elements will endow the resulting optimum beam design with periodicity. The beam elements "a" and "c", together with no more than four other elements, are necessary for the optimization of non-dimensional Bernoulli-Euler beams for any value of *n* and any combination of classical boundary conditions. These elements are all optimized with their designs shown in the first part of Ref. [24], and the elements are listed together with their optimum characteristics in Table 1 of the reference. Finally, very simple explicit algebraic expressions [(30), (57) (63) and (64)] are derived and presented in the reference, for computation of the maximum value of the *n*-th eigenfrequency (in the current example ω_9), of the optimized, assembled beam, and for the proper scaling of the lengths and volumes of the individual, optimized beam elements, such that each of these elements will vibrate at the same frequency as the assembled, optimum beam.

The approach is coined the "Method of Scaled Optimum Beam Elements" [24], and it should be mentioned that for Bernoulli-Euler beams subject to any combination of clamped, simply supported and free end boundary conditions, the geometrically unconstrained optimum solutions to the problem of maximizing the *n*-th eigenfrequency or frequency band-gap corresponding to any value of *n* are available in Ref. [24].

6 FREE WAVE PROPAGATION AND FORCED VIBRATION IN THE OPTIMIZED PERIODIC BEAM STRUCTURE

It is interesting to examine the transverse wave propagation and vibration filter effect in the optimized periodic beam structures obtained in the preceding sections. First, the wave propagation in an infinitely long periodic beam is analyzed, where the infinite beam is constructed by repeated translation of an inner beam segment obtained in the frequency gap optimization above. Subsequently, as an example, a frequency response analysis is conducted for the optimized beam in Fig. 6(b), when the beam is subjected to an external time-harmonic excitation with a view to investigate the attenuation levels in the frequency gap $\Delta\omega_{19} = \omega_{19} - \omega_{18}$.

From the Floquet theory (see [1]) and waveguide finite element (WFE) method [44], the wave propagation through the entire infinite periodic beam mentioned above can be determined by analyzing the wave motion within a single repeated beam segment, which is called a unit cell. The band-gaps can be explored by analyzing the unit cell. The transfer matrix **T** of the unit cell can be defined from the dynamic stiffness matrix of the conventional finite element analysis. Detailed derivation of the transfer matrix is available in [44]. The eigenvalues λ of the transfer matrix **T** are defined by the propagation constant *K* (Bloch

parameter) as [3,45]

$$\lambda = e^{iK} = e^{-K^{\mathrm{Im}}} e^{iK^{\mathrm{Re}}} = e^{-K^{\mathrm{Im}}} \left(\cos\left(K^{\mathrm{Re}}\right) + i \sin\left(K^{\mathrm{Re}}\right) \right), \tag{17}$$

where K^{Re} and K^{Im} represent the real and the imaginary parts of K, respectively. A stop band is found when all eigenvalues λ of $\mathbf{T}$ fulfil the condition $|\lambda| \neq 1$, i.e., $K^{\mathrm{Im}} \neq 0$. In this stop band, free wave propagation is prohibited. Due to two degrees of freedom at each end node of the unit cell, there are four eigenvalues λ_1, λ_2, λ_3, and λ_4 of the transfer matrix.

One of the inner repeated segments in Fig. 3(b) is analyzed as a unit cell in the infinite periodic beam. The magnitude $|\lambda|$ of eigenvalues is plotted as a function of the non-dimensional circular frequency defined in Eq. (1), as shown in Fig. 17, where three stop bands can be identified from the frequency range with $|\lambda| \neq 1$, indicated by three grey domains in Fig. 17. The 8th and 9th non-dimensional circular eigenfrequencies of the uniform, comparison beam and the optimized beam are also shown in Fig. 17. As is well known, no stop band exists in the infinite uniform beam in absence of damping. However, a relatively large stop band for the infinite periodic beam is observed, where bending waves cannot propagate. Similarly, stop bands can be seen in Figs. 18 and 19 for two other examples. These figures demonstrate that there is almost perfect correlation between the band-gap size/location of the emerging band structure and the size/location of the corresponding maximized natural frequency gap in the finite structure.

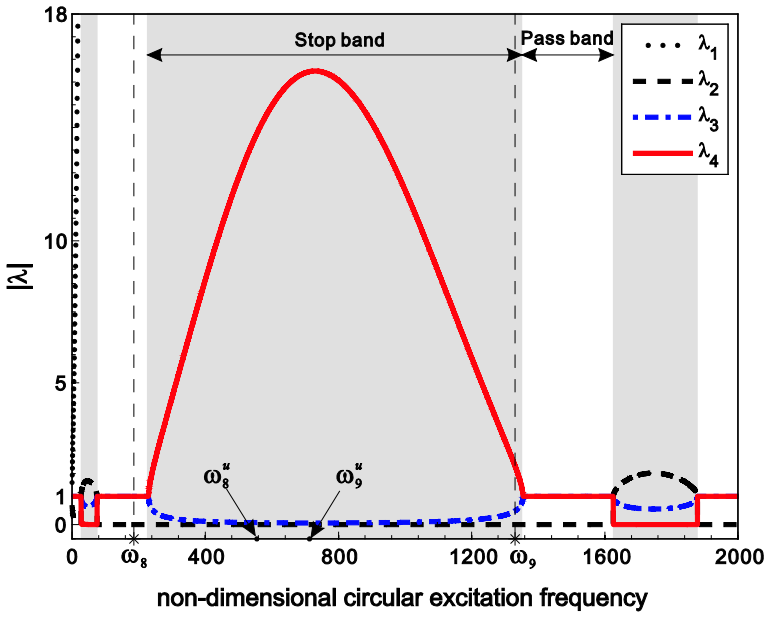

Figure 17: Variation of $|\lambda|$ versus excitation frequency obtained by employing Floquet theory for an inner repeated segment in Fig. 3(b), where the frequency gap $\Delta\omega_9 = \omega_9 - \omega_8$ of the cantilever beam is maximized. The grey domains indicate Floquet-predicted stop bands. The 8th and 9th eigenfrequencies ω_8^u and ω_9^u of the comparison beam with uniform cross-section, and ω_8 and ω_9 of the optimized beam are shown in the figure.

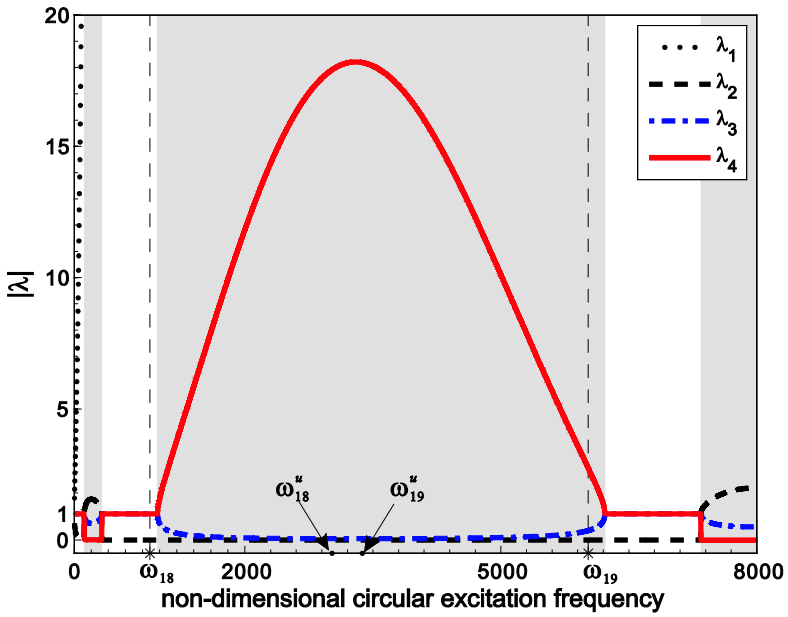

Figure 18: Variation of $|\lambda|$ versus excitation frequency obtained by employing Floquet theory for an inner repeated segment in Fig. 6(b), where the frequency gap $\Delta\omega_{19} = \omega_{19} - \omega_{18}$ of the cantilever beam is maximized. The grey domains indicate Floquet-predicted stop bands. The 18th and 19th eigenfrequencies ω_{18}^{u} and ω_{19}^{u} of the comparison beam with uniform cross-section, and ω_{18} and ω_{19} of the optimized beam are shown in the figure.

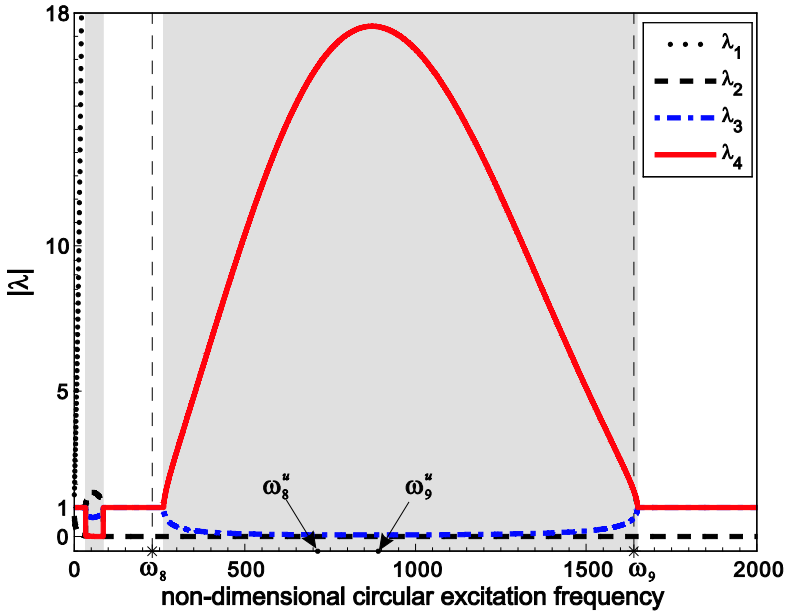

Figure 19: Variation of $|\lambda|$ versus excitation frequency by employing Floquet theory for an inner repeated segment in Fig. 9, where the frequency gap $\Delta\omega_9 = \omega_9 - \omega_8$ of the clamped-clamped beam is maximized. The grey domains indicate Floquet-predicted stop bands. The 8th and 9th eigenfrequencies ω_8^u and ω_9^u of the comparison beam, and ω_8 and ω_9 of the optimized beam are shown in the figure.

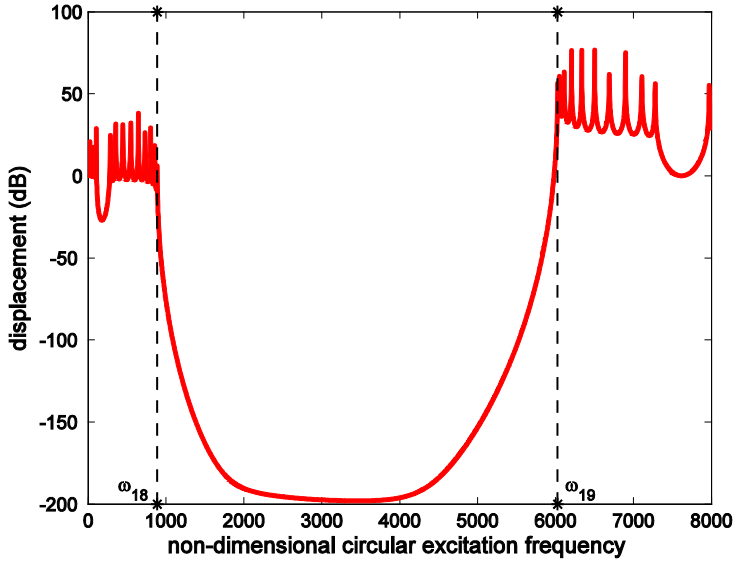

Figure 20: Displacement response at the right hand end from the flexural vibration of the optimized beam in Fig. 6(b) when the beam is subjected to time-harmonic base excitation in the transverse direction at the left hand end. No damping is assumed. The 18th and 19th eigenfrequencies ω_{18} and ω_{19} of the optimized beam are indicated in the figure.

It has been demonstrated in many papers, see e.g. [5,45], that a structure with a finite number of repeated unit cells may significantly suppress propagation of waves with frequencies in the stop band. Fig. 20 shows the displacement response at the right hand end of the optimized beam shown in Fig. 6(b), when the beam is subjected to a time-harmonic base excitation in the transverse direction at the left hand end. The base motion is prescribed with a given displacement amplitude u_0 relative to the fixed reference axis. The transverse displacement u at the right hand end is indicated in Fig. 20 in the form $10\log_{10}\frac{u^2}{u_0^2}$ dB.

It is seen from Fig. 20 that there is a large drop in the response in the stop band frequency range. The stop band calculated from the corresponding unit cell is given in Fig. 18. It demonstrates that the stop band may exist in the optimized beam obtained by maximization of a frequency gap. It is observed from Figs. 18 and 20 that there is a correlation between the value of $|\lambda|$ representing the strength of attenuation in a band gap, and the level of attenuation in the frequency response function for a finite structure composed of the same periodic unit cell. The many resonance peaks observed in Fig. 20 are due to the fact that no damping is included. The resonance peaks can be removed or reduced by including some damping, and we also found that there is no significant change of the band-gap behavior for relatively small damping. The effect of smoothing by including damping is often used in the topology optimization of band-gap structures [7].

7 CONCLUSIONS

Maximizing gaps between two adjacent natural frequencies (eigenfrequencies) of free transverse vibrations of prescribed order is investigated in this paper. The results are obtained by finite element and gradient based optimization using analytical sensitivity analysis. An incremental optimization formulation with consideration of multiple eigenvalues is applied, which can be used for problems with any mix of multiple and simple eigenfrequencies. Non-

dimensional optimum solutions are presented for different classical boundary conditions, different orders of the upper and lower eigenfrequencies of maximized gaps, and values of a minimum cross-sectional area constraint. However, geometrically unconstrained optimum solutions obtained in Ref. [24] are also discussed and utilized in this paper. The results show that, except for beam segments adjacent to the beam ends whose designs are characteristic for the specific boundary conditions considered, all the inner part of the optimum beam designs exhibits a significant periodicity in terms of repeated beam segments, the number of which increases with increasing orders of the upper and lower frequencies of the maximized gaps.

When small values of the minimum cross-sectional area are prescribed, solutions to the current problems are very close to corresponding solutions obtainable by simple non-dimensional analytical expressions for limiting optimum solutions that were derived earlier by a "method of scaled beam elements" [24] in which inner points of vanishing cross-sectional area in the beams were allowed and exploited.

In wave propagation problems, band-gap is found in an infinite beam structure constructed by repeated translation of an inner beam segment obtained by eigenfrequency gap optimization. The band-gap size/location of the emerging band structure is matching very well with the size/location of the corresponding maximized natural frequency gap in the finite structure. For the optimized structures composed of a finite number of repeated segments in the inner part, the motion transmitted from one end will be significantly suppressed by the periodic segments. For the beam structures studied here, it can be concluded that the optimum design maximizing the gap between two adjacent eigenfrequencies of free transverse vibration of given higher order is periodic. It is also demonstrated that the approach tailors a band-gap which is matching very well the maximized frequency gap in the periodic structure characterizing elastic or acoustic wave propagation.

ACKNOWLEDGMENTS

This work was partially supported by the EU InterReg Project "Silent Spaces", Aalborg University, and the National Natural Science Foundation of China (Grant No. 90816025). This support is gratefully acknowledged by the authors.

REFERENCES

[1] L. Brillouin, *Wave Propagation in Periodic Structures, 2nd edition*. Dover Publications. New York, 1953.

[2] M.M. Sigalas, E.N. Economou, Elastic and acoustic-wave band-structure. *Journal of Sound and Vibration*, **158**, 377-382, 1992.

[3] D.J. Mead, Wave propagation in continuous periodic structures: Research contributions from Southampton, 1964-1995. *Journal of Sound and Vibration*, **190**, 495-524, 1996.

[4] J.S. Jensen, O. Sigmund, J.J. Thomsen, M.P. Bendsøe, Design of multi-phase structures with optimized vibrational and wave-transmitting properties. *Proceedings of 15th Nordic Seminar on Computational Mechanics, Aalborg University*. Lund, E., Olhoff, N., Stegmann, J. (Eds). Institute of Mechanical Engineering, Aalborg University, Denmark, p. 63-66, 2002 (ISBN: 87-89206-67-3).

[5] J.S. Jensen, Phononic band gaps and vibrations in one- and two-dimensional mass-spring structures. *Journal of Sound and Vibration*, **266**, 1053-1078, 2003.

[6] M.I. Hussein, G.M. Hulbert, R.A. Scott, Dispersive elastodynamics of 1d banded materials and structures: Analysis. *Journal of Sound and Vibration*, **289**, 779-806, 2006.

[7] O. Sigmund, J.S. Jensen, Systematic design of phononic band-gap materials and structures by topology optimization. *Philosophical Transactions of the Royal Society of London Series A-Mathematical Physical and Engineering Sciences*, **361**, 1001-1019, 2003.

[8] S. Halkjær, O. Sigmund, Optimization of beam properties with respect to maximum band-gap. *Mechanics of the 21st Century, Procedings of 21st International Congress of Theoretical and Applied Mechanics*. Gutkowski, W., Kowalewski, T.A. (Eds.), IUTAM, Warsaw, Poland, 2004 (ISBN: 978-1-4020-3456-5).

[9] A.R. Diaz, A.G. Haddow, L. Ma, Design of band-gap grid structures. *Structural and Multidisciplinary Optimization*, **29**, 418-431, 2005.

[10] M.I. Hussein, K. Hamza, G.M. Hulbert, R.A. Scott, K. Saitou, Multiobjective evolutionary optimization of periodic layered materials for desired wave dispersion characteristics. *Structural and Multidisciplinary Optimization*, **31**, 60-75, 2006.

[11] S. Halkjaer, O. Sigmund, J.S. Jensen, Maximizing band gaps in plate structures, *Structural and Multidisciplinary Optimization*, **32**, 263-275, 2006.

[12] J.S. Jensen, N.L. Pedersen, On maximal eigenfrequency separation in two-material structures: The 1D and 2D scalar cases. *Journal of Sound and Vibration*, **289**, 967-986, 2006.

[13] J.S. Jensen, Topology optimization problems for reflection and dissipation of elastic waves. *Journal of Sound and Vibration*, **301**, 319-340, 2007.

[14] M.I. Hussein, G.M. Hulbert, R.A. Scott, Dispersive elastodynamics of 1D banded materials and structures: Design. *Journal of Sound and Vibration*, **307**, 865-893, 2007.

[15] J.B. Du, N. Olhoff, Topological design of freely vibrating continuum structures for maximum values of simple and multiple eigenfrequencies and frequency gaps. *Structural and Multidisciplinary Optimization*, **34**, 91-110, 2007.

[16] J.B. Du, N. Olhoff, Topological design of freely vibrating continuum structures for maximum values of simple and multiple eigenfrequencies and frequency gaps (vol 34, pg 91, 2007), Editors's Erratum. *Structural and Multidisciplinary Optimization*, **34**, 545-545, 2007.

[17] A.A. Larsen, B. Laksafoss, J.S. Jensen, O. Sigmund, Topological material layout in plates for vibration suppression and wave propagation control. *Structural and Multidisciplinary Optimization*, **37**, 585-594, 2009.

[18] A. Søe-Knudsen, Design of stop-band filter by use of pipe segments and shape optimization. *Structural and Multidisciplinary Optimization*, **44**, 863-874, 2011.

[19] D. Richards, D.J. Pines, Passive reduction of gear mesh vibration using a periodic drive shaft. *Journal of Sound and Vibration*, **264**, 317-342, 2003.

[20] D.L. Yu, Y.Z. Liu, H.G. Zhao, G. Wang, J. Qiu, Flexural vibration band gaps in Euler-Bernoulli beams with locally resonant structures with two degrees of freedom. *Physical Review B*, **73**, 064301, 2006.

[21] L. Liu, M.I. Hussein, Wave motion in periodic flexural beams and characterization of the transition between bragg scattering and local resonance. *Journal of Applied Mechanics*, **79**, 011003-011017, 2012.

[22] A.C. Hladky-Hennion, G. Allan, M. de Billy, Localized modes in a one-dimensional diatomic chain of coupled spheres. *Journal of Applied Physics*, **98**, 054909, 2005.

[23] B.L. Karihaloo, F.I. Niordson, Optimum design of vibrating cantilevers. *Journal of Optimization Theory and Applications*, **11**, 638-654, 1973.

[24] N. Olhoff, Optimization of vibrating beams with respect to higher-order natural frequencies. *Journal of Structural Mechanics*, **4**, 87-122, 1976.

[25] N. Olhoff, Maximizing higher-order eigenfrequencies of beams with constraints on the design geometry. *Journal of Structural Mechanics*, **5**, 107-134, 1977.

[26] N. Olhoff, R. Parbery, Designing vibrating beams and rotating shafts for maximum difference between adjacent natural frequencies. *International Journal of Solids and Structures*, **20**, 63-75, 1984.

[27] M.P. Bendsøe, N. Olhoff, A method of design against vibration resonance of beams and shafts. *Optimal Control Applications & Methods*, **6**, 191-200, 1985.

[28] A.R. Diaz, N. Kikuchi, Solutions to shape and topology eigenvalue optimization problems using a homogenization method. *International Journal for Numerical Methods in Engineering*, **35**, 1487-1502, 1992.

[29] Z.D. Ma, N. Kikuchi, H.C. Cheng, Topological design for vibrating structures. *Computer Methods in Applied Mechanics and Engineering*, **121**, 259-280, 1995.

[30] B. Niu, J. Yan, G. Cheng, Optimum structure with homogeneous optimum cellular material for maximum fundamental frequency. *Structural and Multidisciplinary Optimization*, **39**, 115-132, 2009.

[31] M.P. Bendsøe, O. Sigmund, *Topology optimization: Theory, methods and applications*. Berlin: Springer-Verlag, 2003.

[32] C.S. Jog, Topology design of structures subjected to periodic loading. *Journal of Sound and Vibration*, **253**, 687-709, 2002.

[33] N. Olhoff, J.B. Du, Topological design optimization of vibrating structures. *Proc. The 4th China-Japan-Korea Joint Symposium on Optimization of Structural and Mechanical Systems*, G. Cheng, S. Liu and X. Guo (Eds), Kunming, China, 6-9 November, pp.509-514, 2006.

[34] J.S. Jensen, Topology optimization of dynamics problems with pade approximants. *International Journal for Numerical Methods in Engineering*, **72**, 1605-1630, 2007.

[35] N. Olhoff, B. Niu, G. Cheng, Optimum design of band-gap beam structures. *International Journal of Solids and Structures*, **49**, 3158-3169, 2012.

[36] M. Petyt, *Introduction to finite element vibration analysis, 2nd Ed*. Cambridge University Press, Cambridge, UK, 2010.

[37] M.P. Bendsøe, N. Olhoff, J.E. Taylor, A variational formulation for multicriteria structural optimization. *Journal of Structural Mechanics*, **11**, 523-544, 1983.

[38] N. Olhoff, Multicriterion structural optimization via bound formulation and mathematical programming. *Structural and Multidisciplinary Optimization*, **1**, 11-17, 1989.

[39] A.P. Seyranian, E. Lund, N. Olhoff. Multiple-eigenvalues in structural optimization problems, *Structural Optimization*, **8**, 207-227, 1994.

[40] W.H. Wittrick, Rates of change of eigenvalues, with reference to buckling and vibration problems. *Journal of the Royal Aeronautical Society*, **66**, 590-591, 1962.

[41] W. Zhong, G. Cheng, Second-order sensitivity analysis of multimodal eigenvalues and related optimization techniques. *Journal of Structural Mechanics*, **14**, 421-436, 1986.

[42] K. Svanberg, The method of moving asymptotes - a new method for structural optimization. *International Journal for Numerical Methods in Engineering*, **24**, 359-373, 1987.

[43] E. Lund, *Finite element based design sensitivity analysis and optimization*, Ph.D. Thesis, Special Report No. 23, Dept. of Mechanical Engineering, Aalborg University, Denmark, 1994.

[44] B.R. Mace, D. Duhamel, M.J. Brennan, L. Hinke, Finite element prediction of wave motion in structural waveguides. *Journal of The Acoustical Society of America*, **117**, 2835-2843, 2005.

[45] A. Søe-Knudsen, S.V. Sorokin, Modelling of linear wave propagation in spatial fluid filled pipe systems consisting of elastic curved and straight elements, *Journal of Sound and Vibration*, **329**, 5116-5146, 2010.